

Self-Supervised Enhancement for Depth from a Lightweight ToF Sensor with Monocular Images

Laiyan Ding¹, Hualie Jiang², Jiwei Chen¹, and Rui Huang^{1*}

Abstract—Depth map enhancement using paired high-resolution RGB images offers a cost-effective solution for improving low-resolution depth data from lightweight ToF sensors. Nevertheless, naively adopting a depth estimation pipeline to fuse the two modalities requires groundtruth depth maps for supervision. To address this, we propose a self-supervised learning framework, SelfToF, which generates detailed and scale-aware depth maps. Starting from an image-based self-supervised depth estimation pipeline, we add low-resolution depth as inputs, design a new depth consistency loss, propose a scale-recovery module, and finally obtain a large performance boost. Furthermore, since the ToF signal sparsity varies in real-world applications, we upgrade SelfToF to SelfToF* with submanifold convolution and guided feature fusion. Consequently, SelfToF* maintain robust performance across varying sparsity levels in ToF data. Overall, our proposed method is both efficient and effective, as verified by extensive experiments on the NYU and ScanNet datasets. The code is available at <https://github.com/denyingmx/selftof>.

I. INTRODUCTION

Accurate depth perception is an essential component to a wide range of applications, including visual semantic navigation [1], holistic scene understanding [2], *etc.*. As a result, depth sensors, e.g., Lidar and Time-of-Flight (ToF) cameras, have gained much attention due to their precision and robustness. Nevertheless, they have high prices and energy consumption (e.g., Intel RealSense D435i costs around 300\$ and runs at 7W). As an alternative, lightweight ToF sensors (e.g., ST VL53L5CX [3], dubbed L5) are low-cost and have been used widely in factories for IoT devices. Specifically, L5 only costs less than 5\$ and operates at 0.3w. As a pioneer work, DELTAR [4] have made enhancing the depth map from a L5 with RGB images possible. Depth maps from DELTAR can be further used for other tasks, including Nerf-based SLAM [5]. Note that we regard this task as depth enhancement as it differs from depth superresolution [6], [7] and depth completion [8], [9], in terms of inputs which have extremely low resolution and potential missing zones. Unfortunately, DELTAR still need dense depth groundtruth for supervision, which limits its applications.

To eliminate the burden of collecting groundtruth depth maps for training, we take inspiration from the self-supervised depth estimation methods, e.g., Monodepth2 [10]. These methods can predict depth maps and poses (with the

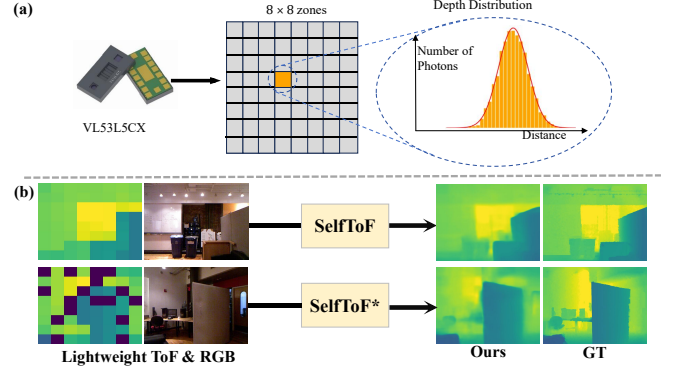


Fig. 1. L5 sensing principle and example inputs and outputs with our SelfToF and SelfToF*. (a) L5 would return zones of resolution 8×8 , and each zone provides depth distribution information. (b) SelfToF and SelfToF* can generate reasonable depth maps in different sparsity setups.

inherent DepthNet and PoseNet) from monocular images without groundtruth supervision. Consequently, we build our SelfToF starting from Monodepth2. We first feed input depth to the DepthNet in addition to the RGB image and design a zone-wise depth consistency loss, as in self-supervised depth completion [11]. Nevertheless, the weight of this depth consistency loss cannot be set high as in previous works due to its imprecise constraint, and the output depth map is still scale-ambiguous. Thus, we introduce a median of median scaling method (MMS), which exploits the zone-wise nature of input depth to recover the metric scale. Consequently, our model is metric-aware and do not need further scaling during testing. Additionally, we propose to feed the input depth to the PoseNet for better pose and depth estimation. Overall, these ingredients allow a large performance boost.

To cope with invalid or missing zones (similar to different sparsity levels in depth completion [12]), we introduce SelfToF*, which replaces the depth encoder in SelfToF with a submanifold one and adds a guided feature fusion module to mitigate performance drop due to the sparsity. This way, the propagation of the input depth feature is carefully controlled and leads to the robustness of SelfToF*. Example inputs and outputs of SelfToF and SelfToF* are in Fig. 1 (b). Compared with the baseline Monodepth2, SelfToF reduce abs_rel from 0.154 to 0.049. Furthermore, SelfToF* retain the abs_rel of 0.053 while SelfToF rise to 0.060.

Our contributions can be summarized as follows. Firstly, we propose SelfToF, a self-supervised framework that can enhance the depth map from a lightweight ToF sensor

*Corresponding author

¹Laiyan Ding, Jiwei Chen and Rui Huang are with School of Science and Engineering, The Chinese University of Hong Kong, Shenzhen 518172, China (e-mail: laiyanding@link.cuhk.edu.cn; jiweichen2@link.cuhk.edu.cn; ruihuang@cuhk.edu.cn).

²Hualie Jiang is with Insta360 Research, Shenzhen 518000, China (e-mail: jianghualie@insta360.com).

with paired images. Secondly, quantitative and qualitative results verify that SelfToF performs better than previous architectures designed for self-supervised estimation [10], [13], or guided depth upsampling [14]. Lastly, we introduce a submanifold depth encoder and guided feature fusion to upgrade from SelfToF to SelfToF*, which is more robust to sparsity variation from the lightweight ToF sensor.

II. RELATED WORKS

A. Self-Supervised Monocular Depth Estimation

These approaches do not require depth ground truth [15] or rectified stereo pairs [16] for end-to-end depth learning. Instead, they learn the depth and inter-frame poses simultaneously [17]. The supervisory signal originates from the assumed photometric consistency between the given current frame and the reconstructed current frame from temporally adjacent frames. Thus, the depth and pose networks can learn end-to-end with only monocular images. Later on, great efforts including devising heuristic loss functions [18], [10], [17], improving robustness to moving objects [19], [20], extending to modern surround applications [21], [22], [23] and designing efficient networks [24], [25]. These works mostly focus on problems in outdoor and autonomous driving scenarios, while another line of research pays attention to challenges rooted in indoor scenes. The progress that tackles textureless regions and large rotations has been made [13], [26], [27], [28], [29]. More importantly, these methods based on monocular images can predict depth maps with high resolution and rich details. Thus, we aim to enhance the low-resolution depth map from a lightweight ToF sensor with this self-supervised learning paradigm.

B. Self-Supervised Monocular Depth Completion

Ma *et al.* propose a self-supervised depth completion framework [11] that requires only sparse depth and paired RGB images as inputs and supervision during training or testing. Later, VOICED [30] explores how to use SLAM systems with self-supervised depth completion. KBNNet [31] design a sparse-to-dense module that densifies sparse depth input and a Calibrated Backprojection Layer which can inject spatial positional encoding into the network. SelfDeco [32] employs a deep stack of sparse convolution layers [33] and pixel adaptive convolution [34] to fuse features from different modalities. Mondri [35] investigates how to effectively learn from a blind ensemble of teacher models by using photometric reconstruction errors as the criterion. Differently, our model takes a low-resolution depth map as input rather than a sparse depth map. Moreover, we introduce a submanifold depth encoder and a guided feature fusion to mitigate performance drop in different ToF sparsity levels.

C. Lightweight-ToF-based Depth Estimation

DELTAR [4] predicts a high-resolution depth map given paired RGB image and low-resolution depth information from a lightweight ToF sensor. The produced depth map can help develop the SLAM system [5] which is based on NeRF [36]. Ours is a self-supervised framework that can be trained

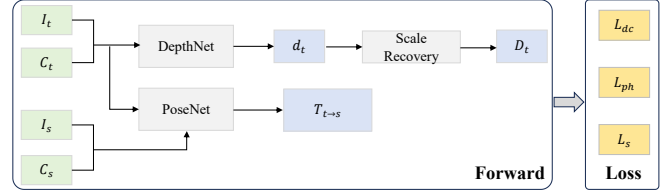


Fig. 2. Training pipeline of our model. During forward, the model takes paired RGB images and low-resolution depth maps from L5 as inputs and outputs depth maps for the current frame and the relative pose between the current frame and source frame. Then, the loss functions, including depth consistency loss (L_{dc}), photometric loss (L_{ph}), and smoothness loss (L_s), can be computed to supervise the DepthNet and PoseNet jointly.

end-to-end without groundtruth depth as supervision. This advantage of our system allows more potential applications, similar to self-supervised depth estimation [10], [17].

III. METHOD

Similar to self-supervised depth estimation [10], our task of self-supervised enhancement for a depth map from a lightweight ToF sensor with images requires a DepthNet and a PoseNet. Both methods are trained on multiple temporally adjacent frames without depth groundtruth supervision. Differently, our model takes additional paired depth maps from lightweight ToF sensors as inputs and produces scale-aware depth output rather than scale-ambiguous ones [17].

In the following, we first briefly introduce the sensing mechanism of the lightweight ToF sensor, e.g., L5 [3]. Then, we illustrate the overall framework of our SelfToF, which takes inspiration from self-supervised depth estimation and completion [11]. Lastly, we describe our additional designs containing submanifold depth encoder and guided feature fusion, which can mitigate the performance drop of our model given different sparsities of ToF signals, i.e., zeros in the input low-resolution depth map.

A. Sensing Mechanism of L5

As mentioned above, L5 is low-cost and low-energy compared with traditional depth sensors, e.g., RealSense and Kinect V2. Nevertheless, it has a very low resolution of only 8×8 (64 zones in total), and each zone measures the depth distribution of its corresponding scene in the 3D scene. Specifically, as depicted in Fig. 1 (a), the L5 sensor evaluates depth by counting photons received within specific time frames. This data is then approximated using a Gaussian distribution, allowing the sensor to transmit only the mean and variance [4]. In this work, we would take these Gaussians' mean as inputs, forming a depth map of resolution 8×8 .

B. Overall Framework

Assuming that L5 zones are aligned with RGB images and no maximum distance constraint exists, then the training pipeline of SelfToF is illustrated in Fig. 2. SelfToF takes low-resolution depth maps (C_t, C_s) from a lightweight ToF sensor and paired RGB images (I_t, I_s) as inputs, where t and s are

the indexes of the target frame and the source frame. The DepthNet can generate a scale-ambiguous depth output d_t , which can be further transformed to metric-aware D_t through our scale-recovery module. The PoseNet takes paired images and depth maps as inputs and outputs the relative pose $T_{t \rightarrow s}$ between the target frame and the source frame. Lastly, we calculate the overall loss function as the weighted summation among the depth consistency loss (L_{dc}), photometric loss (L_{ph}), and smoothness loss (L_s). Note that, during testing, only DepthNet is required to perform depth enhancement.

1) *DepthNet*: The DepthNet consists of an RGB encoder, a depth encoder, a fusion module, and a decoder, as in Fig. 3 (a). The RGB encoder is a ResNet18 [37] initialized from ImageNet [38] pretrained weights. The depth encoder is a simple network that contains multiple 1×1 and 3×3 convolution layers and operates on the 8×8 resolution without downsampling. The RGB encoder outputs feature maps of different resolutions, while ToF encoders produce the same number of feature maps of the same spatial size. Then paired feature maps are fused (addition or guided feature fusion in Sec. III-D.2) and passed to the lightweight decoder, which has consecutive convolution and upsampling operations, as in Monodepth2. Note that if we use addition as the fusion between depth and RGB features, compared with Monodepth2, the Multiply-Accumulate Operations (MACs) only increase from 2.38G to 2.59 G. Consequently, SelfToF is efficient as it can run at more than 100 FPS with a single RTX2080Ti GPU with a RGB resolution of 256×256 .

2) *PoseNet*: The PoseNet also includes an RGB encoder, a depth encoder, a fusion module, and a decoder, as in Fig. 3 (b). The process is similar to DepthNet, except only the feature maps at the lowest level are fused and decoded for rotation and translation. Though previous works [11], [31], [32] have tried different ways to estimate the relative temporal pose, they only use the RGB information. Differently, we utilize the input depth information for better pose estimation. This small modification allows a large performance boost as validated by Table I.

3) *Scale Recovery*: Following prior self-supervised depth completion works, we design a depth consistency loss L_{dc} (Eq. 6) to maintain the consistency of output and input depth. Differently, L_{dc} is a zone-wise loss function instead of a point-wise loss. Consequently, we notice that assigning a large weight to L_{dc} (e.g., 1.0) as previous works [11] will force the output to be too similar to the input depth. Furthermore, the other two loss functions, L_{ph} and L_s , cannot help reveal the metric scale. Thus, simply lowering the weight of L_{dc} cannot guarantee that the output depth is scale-aware. To this end, we propose a scale-recovery module to recover the actual scale without increasing the weight of L_{dc} .

A naive way is to conduct median scaling similar to the median scaling (MS) in the self-supervised depth estimation evaluation protocol [17]. That is,

$$D_t = \frac{\text{median}(C_t)}{\text{median}(d_t)} * d_t \quad (1)$$

This is indeed useful but does not consider the zone-wise

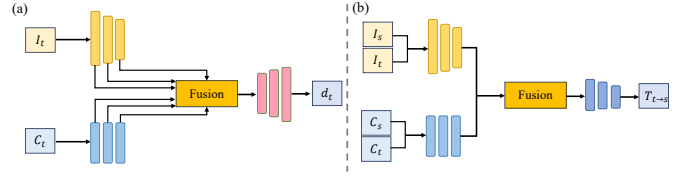


Fig. 3. Overview of multi-modality DepthNet and PoseNet. The fusion is a simple addition fusion and our guided feature fusion in SelfToF and SelfToF*, respectively.

nature of ToF signals. Thus, we can first obtain the zone-wise scales and then take the median of these scales as the final overall scale. That is,

$$D_t = \text{median}\left(\left\{\frac{C_t^i}{\text{median}(d_t^i)}\right\}\right) * d_t \quad (2)$$

where C_t^i and d_t^i are the i th zone in C_t and d_t . Moreover, we name this as the median of median scaling (MMS).

C. Loss Functions

1) *Photometric Loss*: With the camera intrinsic matrix K , the relative pose $T_{t \rightarrow s}$, and the depth of the current frame D_t , we can synthesize the current frame $I_{s \rightarrow t}$ from the source frame with backward warping. Same as previous works, this synthesis follows:

$$I_{s \rightarrow t}(x) = I_s(\text{proj}(D_t, K, T_{t \rightarrow s})). \quad (3)$$

where $\text{proj}()$ calculates the resulting 2D coordinates in the source image, $\langle \rangle$ is the bilinear sampling function [39] for non-integer pixel coordinates.

Then the photometric loss L_{ph} is the weighted sum of the L1 loss and the SSIM loss [40]:

$$L_{ph}(I_t, I_{s \rightarrow t}) = \alpha \frac{1 - \text{SSIM}(I_t, I_{s \rightarrow t})}{2} + (1 - \alpha) \|I_t - I_{s \rightarrow t}\|, \quad (4)$$

where α is conventionally set to be 0.85.

2) *Smoothness Loss*: Following previous works, we also include a smoothness loss L_s to exploit the textures from the RGB image for depth estimation:

$$L_s = |\partial_x d_t^*| e^{-|\partial_x d_t|} + |\partial_y d_t^*| e^{-|\partial_y d_t|}, \quad (5)$$

where ∂_x and ∂_y represent the gradients along the x and y direction. d_t^* is the mean normalized disparity [41] to prevent the shrinking of predicted disparity.

3) *Depth Consistency Loss*: Since a lightweight ToF sensor can provide the mean μ_i and standard deviation σ_i of fitted Gaussian distribution of the histogram for the i th zone [4], we conduct this procedure for the predicted depth map to get $\tilde{\mu}_i$ and $\tilde{\sigma}_i$. Then our depth consistency loss L_{dc} is defined as the distance between two 1D Gaussian distributions [42]:

$$L_{dc} = \sum_i (\mu_i - \tilde{\mu}_i)^2 + (\sigma_i - \tilde{\sigma}_i)^2, \quad (6)$$

Notice that this equation can still be applied without the Gaussian assumption since it penalizes the differences between the two sets of mean and standard deviation.

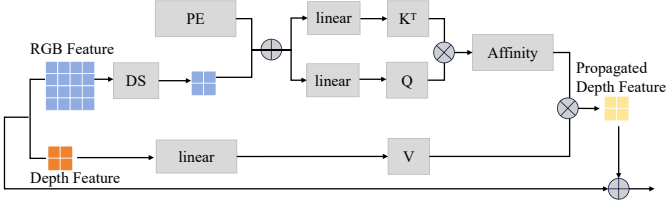


Fig. 4. Overview of guided feature fusion. We first downsample (DS) RGB features and add position encoding [47] to it. Then, an affinity map is calculated to help propagate ToF features. Finally, the output of this module is the summation of the original RGB features, depth features, and propagated depth features. Resizing and flattening are omitted for simplicity.

4) *Overall Loss Function:* Our final loss for training is:

$$L = w_{ph}L_{ph} + w_sL_s + w_{dc}L_{dc}, \quad (7)$$

where w_{ph} , w_s , and w_{dc} are empirically set as 1.0, 0.1, and 0.01.

D. Techniques to tackle with Sparsity in ToF

Similar to prior studies on depth completion [9], [31], we conduct experiments where the sparsity of ToF varies by setting some of the zones as invalid or missing and filling them with zeros. As expected, the depth prediction performance in both valid and invalid zones suffers from drops. We argue that during depth feature encoding, valid zones may gather useless information from invalid zones and invalid zones cannot gather most related features from valid zones correctly. Thus, proper control over the depth feature propagation is essential to mitigate the performance drop due to invalid zones. To this end, we introduce a submanifold depth encoder and a guided feature fusion module to upgrade SelfToF to SelfToF*, which suffers from less performance drop when some zones are invalid in the input depth map.

1) *Submanifold Depth Encoder:* We turn the conventional depth feature encoder into a submanifold depth encoder by replacing all layers with their submanifold versions [43] implemented by Spconv [44]. This way, the valid zones will gather information from only valid zones, and invalid zones will remain zeros. Different from previous works that use sparsity invariant convolution layers [32], [33] for better performance, we use submanifold layers [43] for preventing uncontrolled depth feature propagation. Also, we validate that this submanifold encoder is necessary for guided feature fusion to be effective in Table V.

2) *Guided Feature Fusion:* When there is no sparsity in ToF, we use addition to fuse RGB and depth features. Nevertheless, when the sparsity exists, we aim to first propagate depth features under the guidance of RGB features and pixel positions. This allows the invalid zones to collect most related features from other zones and better fusion. To realize this intuition, we take inspiration from affinity-based methods [45], [46] and self-attention [47].

Specifically speaking, as illustrated in Fig. 4, given RGB and depth features, we first downsample the RGB feature to the resolution of the depth feature and flatten both the low-resolution RGB and depth features. Then, after the position

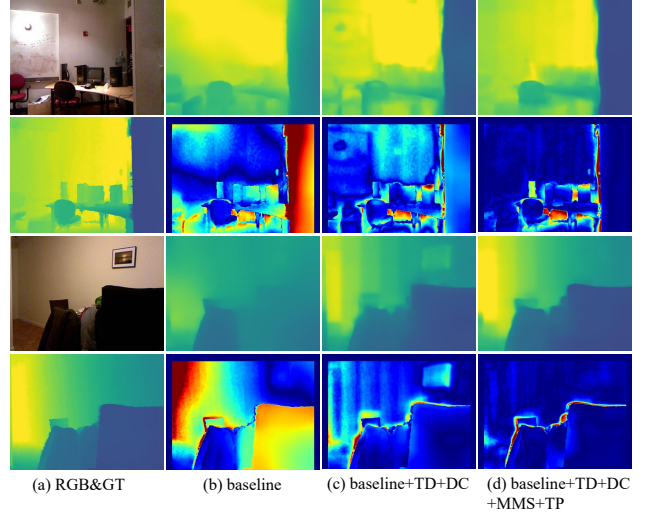


Fig. 5. Visual results and error maps on the NYU dataset. Using ToF as DepthNet inputs (TD) and depth consistency loss (DC) can help recover better geometry. Furthermore, superior performance can be achieved with median of median scaling (MMS) and using ToF as PoseNet inputs (TP).

embedding [47] is added to the low-resolution RGB features, two linear layers are responsible for generating the key (K^T), which is transposed, and value (Q) tensors. With a multiplication between the transposed key and value, we obtain the affinity matrix that is both semantic-aware and position-aware. Next, this affinity matrix propagates the generated value tensor from depth features through another matrix multiplication. Lastly, this module outputs the summation of the RGB feature, the propagated depth feature, and the original depth feature. Since this module operates on the 8×8 resolution, it brings little computation burden to the whole network.

IV. EXPERIMENTS

In this section, we first describe the dataset preparation, implementation details, and evaluation metrics. Then, we provide results to validate our designs while building SelfToF. Lastly, we verify that our submanifold depth encoder and guided feature fusion can mitigate performance drops in various sparsity setups.

A. Dataset Preparation

As for the dataset preparation, we follow previous works [13] to sample one target frame every five frames and obtain training sets of size 47K from the NYU dataset [48]. The source frames are selected by sampling the ± 10 frames around the target frame so that enough translation exists between source and target frames [26]. To simulate the ToF signal from a lightweight ToF sensor, e.g., L5, we follow the process in DELTAR [4] to fit the histogram for each zone with a Gaussian distribution. For evaluation, we test on the official 654 samples with single-frame RGB input and paired ToF depth map. As for studies on the sparsity of ToF, we randomly fill some of the low-resolution depth maps with

zeros. Notice that our SelfToF is scale-aware while previous self-supervised depth estimation is scale-ambiguous. Also, We conduct median scaling for the evaluation of scale-ambiguous methods.

B. Implementation Details

We implement our SelfToF with Pytorch [49]. For training, we use the Adam optimizer [50] with $\beta_1 = 0.9, \beta_2 = 0.999$. The learning rate is $1 \times e^{-4}$ for the first 30 epochs and remains $1 \times e^{-5}$ for the rest 10 epochs. The network is trained on four NVIDIA RTX 2080Ti GPUs with a batchsize of 8 on each GPU, which takes around 12 hours in total. The resolution of the RGB image and the depth map from a lightweight ToF sensor are 256×256 and 8×8 , respectively.

C. Evaluation Metrics

We follow previous works [26], [51] to report standard metrics for depth prediction, including absolute relative error (abs_rel), squared relative difference (sq_rel), root mean squared error (rmse), rmse_log, log₁₀ error and threshold accuracy (δ_i).

TABLE I
ABLATION OF COMPONENTS IN SELFToF ON NYU DATASET. BEST PERFORMANCE AMONG SELF-SUPERVISED METHODS IS **BOLDED**.

	SA	abs_rel	sq_rel	rmse	rmse_log	log10	a1	a2	a3
baseline	No	0.154	0.123	0.574	0.196	0.065	0.788	0.951	0.987
+TD	No	0.098	0.061	0.420	0.132	0.042	0.907	0.985	0.996
+TD+DC	No	0.085	0.044	0.354	0.118	0.037	0.932	0.989	0.998
+TD+DC+MS	Yes	0.078	0.041	0.343	0.121	0.035	0.933	0.986	0.996
+TD+DC+MMS	Yes	0.071	0.037	0.323	0.113	0.032	0.942	0.988	0.997
+TD+DC+MMS+TP	Yes	0.049	0.029	0.282	0.091	0.022	0.960	0.990	0.997
baseline+TD+S	Yes	0.046	0.023	0.230	0.080	0.019	0.964	0.993	0.998

D. Building SelfToF

We start from a baseline self-supervised depth estimation framework, a single-scale MonoDepth2. Then, we add ToF as DepthNet inputs (TD), use depth consistency loss (DC), apply scale recovery (MS and MMS), and add ToF as PoseNet inputs (TP) sequentially, resulting in the final SelfToF.

As listed in Table I, adding TD and DC to the baseline can boost the performance, similar to previous self-supervised depth completion methods [11], [30]. Nevertheless, the results are still not scale-aware (SA) as we cannot set a large weight to L_{dc} . Consequently, we propose to find the actual scale by comparing the input ToF and predicted depth with MS and MMS. Both MS and MMS can recover the scale, yet MMS can lead to better numerical results since it exploits the zone-wise nature of lightweight ToF. Lastly, we find that using ToF as PoseNet inputs (TP) can additionally lead to a substantial performance increase. Overall, compared with the baseline method, we can reduce the abs_rel and sq_rel by 68.2% and 76.4%, respectively. Additionally, we train a baseline with TD and groundtruth supervision (S), and the result is in the last row. We can see only a small gap between SelfToF and this supervised model in most metrics.

Additionally, visual results on building SelfToF are given in Fig. 5. With TD and DC, the model can perform much better in areas where the photometric supervision is insufficient, e.g., low-light or over-exposed areas. Furthermore,

an even greater performance boost can be realized with our proposed MMS and TP.

E. Comparison with other methods

We provide quantitative and qualitative results to examine the superior performance of SelfToF compared with other related methods, including MonoDepth2, nearest neighbour upsampling (NN), and guided filter (GF) [14].

As shown in Table II, our SelfToF achieve the best performance among similar methods. Concretely, SelfToF outperform GF [14] by reducing sq_rel from 0.041 to 0.029, which is a 29.3% reduction.

We also visualize the results that different methods obtain in Fig. 6. Since we take advantage of self-supervised depth estimation, SelfToF can produce depth maps much sharper than nearest upsampling and guided filter [14]. Additionally, SelfToF predicts more accurate output than MonoDepth2 as it exploits the depth information from ToF.

These quantitative and qualitative results indicate that SelfToF fully exploits the information from RGB images and depth maps from lightweight ToF sensors. Furthermore, SelfToF can output reasonable depth maps when sparsity in ToF exists. Traditional methods like NN and GF [14] may fail in this case.

TABLE II
QUANTITATIVE COMPARISON AMONG SELFToF, MONODEPTH2, NEAREST NEIGHBOUR UPSAMPLING (NN), AND GUIDED FILTER (GF).

	SA	abs_rel	sq_rel	rmse	rmse_log	log10	a1	a2	a3
MonoDepth2	No	0.154	0.123	0.574	0.196	0.065	0.788	0.951	0.987
NN	Yes	0.070	0.064	0.405	0.140	0.031	0.926	0.970	0.988
GF	Yes	0.058	0.041	0.345	0.113	0.027	0.937	0.982	0.994
SelfToF	Yes	0.049	0.029	0.282	0.091	0.022	0.960	0.990	0.997

F. Generalization on ScanNet

Following prior works [26], [13], we evaluate the depth estimation and pose estimation on ScanNet [52] with the NYU [48] trained model. The results are listed in Table III. In addition to achieving much better depth-related results, SelfToF obtain smaller rotational error (rot) and translational angular error (tr). One may refer to SC-DepthV2 [28] or MonoIndoor [53] for even better pose estimation. Moreover, we find that SelfToF even generalize better than a supervised version of the baseline.

TABLE III
GENERALIZATION RESULTS ON SCANNET[52].

	SA	abs_rel	sq_rel	rmse	rmse_log	log10	a1	rot(deg)	tr(deg)
baseline	No	0.181	0.109	0.439	0.225	0.076	0.724	1.740	32.770
SelfToF	Yes	0.044	0.015	0.169	0.084	0.020	0.966	1.521	28.217
baseline+TD+S	Yes	0.068	0.022	0.168	0.101	0.027	0.933	-	-

G. Handling the sparsity in ToF

To investigate how sparsity in ToF influences the model performance, we train and test our SelfToF with ToF randomly missing. That is, we fill some zones with zeros randomly.

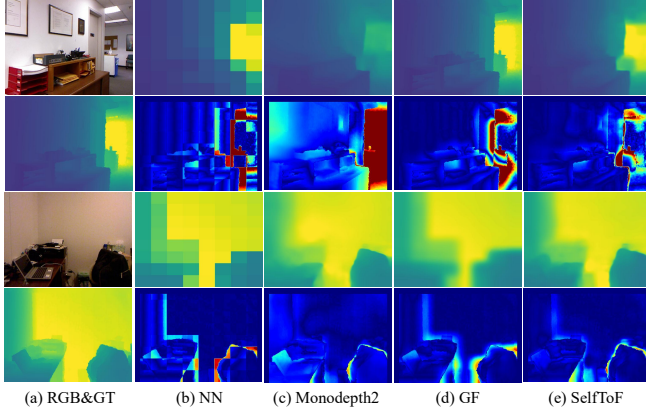


Fig. 6. Visual results and error maps on NYU dataset. Compared with nearest upsampling (b), Monodepth2 (c), guided filter (d), our SelfToF (e) can produce depth maps with smaller errors and sharper object boundaries.

As listed in Table IV, when the sparsity rate (SR) increases, SelfToF obtain worse results on all metrics consistently. We argue that the zero-value zones originated from sparsity in the lightweight ToF sensor leads to wrong feature propagation during depth feature encoding.

Consequently, we propose SelfToF* based on SelfToF by manipulating the depth feature encoding and propagation effectively. This upgrade is realized by using a submanifold depth encoder and a guided feature propagation module. By comparing the results from SelfToF* and SelfToF in Table IV, we observe that SelfToF* achieve better performance in different sparsity settings.

TABLE IV

COMPARISON BETWEEN SELFTOF AND SELFTOF* UNDER DIFFERENT SPARSITY RATIOS (SR).

	SR	abs_rel	sq_rel	rmse	rmse_log	log10	a1	a2	a3
SelfToF	0.0	0.049	0.029	0.282	0.091	0.022	0.960	0.990	0.997
SelfToF	0.2	0.060	0.034	0.305	0.100	0.026	0.952	0.989	0.997
SelfToF	0.4	0.070	0.042	0.337	0.111	0.031	0.939	0.987	0.997
SelfToF*	0.0	0.049	0.029	0.281	0.090	0.022	0.961	0.990	0.997
SelfToF*	0.2	0.053	0.031	0.291	0.095	0.024	0.957	0.990	0.997
SelfToF*	0.4	0.061	0.036	0.314	0.104	0.027	0.949	0.988	0.997

Furthermore, we provide more results to verify why using a Submanifold Depth Encoder (SDE) is necessary and how our Guided Feature Fusion (GFF) works.

First, looking at Table V where the results are obtained with 20% sparsity, we observe that (1) using SDE does not lead to a performance boost. (2) GFF obtain much better results with SDE than used alone. These results indicate that a submanifold depth encoder is necessary to prevent improper feature propagation and allow better feature propagation in later stages. This differs from previous works [33], [32] that use sparsity invariant convolution layers for only performance improvement.

Second, we visualize obtained affinity maps in Fig. 7. The zones with red boundaries are valid, while those with black boundaries are invalid. For the invalid blue zone, its associated affinity map or attention map is in the first row in Fig. 7 (d). The similarity map concentrates at zones that

TABLE V

ABLATION STUDIES OF UPGRADING SELFTOF TO SELFTOF*.

	abs_rel	sq_rel	rmse	rmse_log	log10	a1	a2	a3
SelfToF	0.060	0.034	0.305	0.100	0.026	0.952	0.989	0.997
+SDE	0.060	0.034	0.304	0.100	0.026	0.953	0.989	0.997
+GFF	0.057	0.034	0.307	0.100	0.025	0.953	0.989	0.997
+SDE+GFF	0.053	0.031	0.291	0.095	0.024	0.957	0.990	0.997

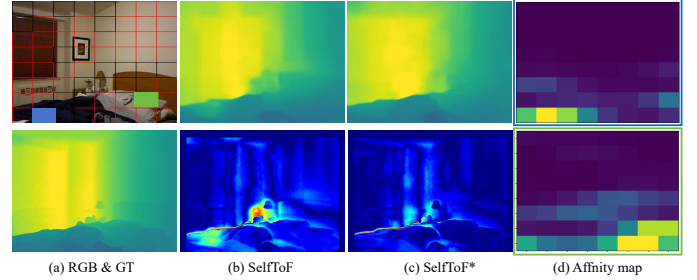


Fig. 7. Visual results and error maps SelfToF and SelfToF* obtain. When some of the ToF is missing, SelfToF* can achieve lower errors in both valid zones and invalid zones. Also, the affinity map indicate that our guided feature fusion can indeed help propagate depth features correctly.

belong to the same quilt. Similarly, the valid green zone has larger similarities with zones that are subject to the same pillow, as shown in the second row in Fig. 7. Additionally, SelfToF* achieves lower errors in these two regions. These results validate the effectiveness of our proposed feature fusion and give a visual explanation of why it can help propagation features correctly.

Additionally, we study how the downsampling choice would affect the final performance. Specifically, given SelfToF with a submanifold depth encoder equipped, we ablate with regular convolution, depthwise convolution, and average pooling and present the results in Table VI. We find that using average pooling can perform best, and fortunately, it is the most efficient one as no other parameters are required.

TABLE VI

ABLATION STUDIES ON THE CHOICE OF DOWNSAMPLING STRATEGIES IN GUIDED FEATURE FUSION.

Downsample Type	abs_rel	sq_rel	rmse	rmse_log	log10	a1	a2	a3
Conv	0.053	0.031	0.294	0.097	0.024	0.956	0.989	0.997
Depthwise Conv	0.055	0.032	0.296	0.096	0.024	0.956	0.990	0.997
Avg Pooling	0.053	0.031	0.291	0.095	0.024	0.957	0.990	0.997

V. CONCLUSIONS

In this work, we propose SelfToF, a method that can enhance the low-resolution depth map from a lightweight ToF sensor with its paired RGB image. Furthermore, we build SelfToF* upon SelfToF by using a submanifold depth encoder and guided feature fusion to mitigate the performance drop due to the sparsity in ToF.

For future work, one may consider collecting large-scale real-world datasets to facilitate studies on challenges rooted in real scenarios for lightweight ToF applications. Additionally, incorporating lightweight ToF sensors with depth foundation models [54], [55] to achieve generalized metric depth estimation results [56] could be promising.

REFERENCES

- [1] Y. Liang, B. Chen, and S. Song, "Sscnav: Confidence-aware semantic scene completion for visual semantic navigation," in *2021 IEEE international conference on robotics and automation (ICRA)*. IEEE, 2021, pp. 13 194–13 200.
- [2] T. Wang, X. Mao, C. Zhu, R. Xu, R. Lyu, P. Li, X. Chen, W. Zhang, K. Chen, T. Xue, *et al.*, "Embodiedscan: A holistic multi-modal 3d perception suite towards embodied ai," in *Proceedings of the IEEE/CVF Conference on Computer Vision and Pattern Recognition*, 2024, pp. 19 757–19 767.
- [3] "Stmicroelectronics: Time-of-flight (tof) 8x8 multizone ranging sensor with wide field of view." [Online]. Available: <https://www.st.com/en/imaging-and-photonics-solutions/vl5315cx.html>
- [4] Y. Li, X. Liu, W. Dong, H. Zhou, H. Bao, G. Zhang, Y. Zhang, and Z. Cui, "Deltar: Depth estimation from a light-weight tof sensor and rgb image," in *European conference on computer vision*. Springer, 2022, pp. 619–636.
- [5] X. Liu, Y. Li, Y. Teng, H. Bao, G. Zhang, Y. Zhang, and Z. Cui, "Multi-modal neural radiance field for monocular dense slam with a light-weight tof sensor," in *Proceedings of the IEEE/CVF international conference on computer vision*, 2023, pp. 1–11.
- [6] Z. Wang, Z. Yan, and J. Yang, "Sgnet: Structure guided network via gradient-frequency awareness for depth map super-resolution," in *Proceedings of the AAAI Conference on Artificial Intelligence*, vol. 38, no. 6, 2024, pp. 5823–5831.
- [7] L. He, H. Zhu, F. Li, H. Bai, R. Cong, C. Zhang, C. Lin, M. Liu, and Y. Zhao, "Towards fast and accurate real-world depth super-resolution: Benchmark dataset and baseline," in *Proceedings of the IEEE/CVF Conference on Computer Vision and Pattern Recognition*, 2021, pp. 9229–9238.
- [8] J. Park, K. Joo, Z. Hu, C.-K. Liu, and I. So Kweon, "Non-local spatial propagation network for depth completion," in *Computer Vision—ECCV 2020: 16th European Conference, Glasgow, UK, August 23–28, 2020, Proceedings, Part XIII 16*. Springer, 2020, pp. 120–136.
- [9] Y. Zhang, X. Guo, M. Poggi, Z. Zhu, G. Huang, and S. Mattoccia, "Completionformer: Depth completion with convolutions and vision transformers," in *Proceedings of the IEEE/CVF conference on computer vision and pattern recognition*, 2023, pp. 18 527–18 536.
- [10] C. Godard, O. Mac Aodha, M. Firman, and G. J. Brostow, "Digging into self-supervised monocular depth estimation," in *Proceedings of the IEEE/CVF international conference on computer vision*, 2019, pp. 3828–3838.
- [11] F. Ma, G. V. Cavalheiro, and S. Karaman, "Self-supervised sparse-to-dense: Self-supervised depth completion from lidar and monocular camera," in *2019 International Conference on Robotics and Automation (ICRA)*. IEEE, 2019, pp. 3288–3295.
- [12] Y. Long, H. Yu, and B. Liu, "Depth completion towards different sensor configurations via relative depth map estimation and scale recovery," *Journal of Visual Communication and Image Representation*, vol. 80, p. 103272, 2021.
- [13] H. Jiang, L. Ding, J. Hu, and R. Huang, "Plnet: Plane and line priors for unsupervised indoor depth estimation," in *2021 International Conference on 3D Vision (3DV)*. IEEE, 2021, pp. 741–750.
- [14] K. He, J. Sun, and X. Tang, "Guided image filtering," *IEEE transactions on pattern analysis and machine intelligence*, vol. 35, no. 6, pp. 1397–1409, 2012.
- [15] H. Fu, M. Gong, C. Wang, K. Batmanghelich, and D. Tao, "Deep ordinal regression network for monocular depth estimation," in *Proceedings of the IEEE conference on computer vision and pattern recognition*, 2018, pp. 2002–2011.
- [16] R. Garg, V. K. Bg, G. Carneiro, and I. Reid, "Unsupervised cnn for single view depth estimation: Geometry to the rescue," in *Computer Vision—ECCV 2016: 14th European Conference, Amsterdam, The Netherlands, October 11–14, 2016, Proceedings, Part VIII 14*. Springer, 2016, pp. 740–756.
- [17] L. Zhou, J. Ye, M. Abello, S. Wang, and M. Kaess, "Unsupervised learning of monocular depth estimation with bundle adjustment, super-resolution and clip loss," *arXiv preprint arXiv:1812.03368*, 2018.
- [18] J. Bian, Z. Li, N. Wang, H. Zhan, C. Shen, M.-M. Cheng, and I. Reid, "Unsupervised scale-consistent depth and ego-motion learning from monocular video," *Advances in neural information processing systems*, vol. 32, 2019.
- [19] H. Jiang, L. Ding, Z. Sun, and R. Huang, "Unsupervised monocular depth perception: Focusing on moving objects," *IEEE Sensors Journal*, vol. 21, no. 24, pp. 27 225–27 237, 2021.
- [20] V. Casser, S. Pirk, R. Mahjourian, and A. Angelova, "Depth prediction without the sensors: Leveraging structure for unsupervised learning from monocular videos," in *Proceedings of the AAAI conference on artificial intelligence*, vol. 33, no. 01, 2019, pp. 8001–8008.
- [21] J.-H. Kim, J. Hur, T. P. Nguyen, and S.-G. Jeong, "Self-supervised surround-view depth estimation with volumetric feature fusion," *Advances in Neural Information Processing Systems*, vol. 35, pp. 4032–4045, 2022.
- [22] L. Ding, H. Jiang, J. Li, Y. Chen, and R. Huang, "Towards cross-view-consistent self-supervised surround depth estimation," *arXiv preprint arXiv:2407.04041*, 2024.
- [23] Y. Wei, L. Zhao, W. Zheng, Z. Zhu, Y. Rao, G. Huang, J. Lu, and J. Zhou, "Surrounddepth: Entangling surrounding views for self-supervised multi-camera depth estimation," in *Conference on robot learning*. PMLR, 2023, pp. 539–549.
- [24] A. Karpov and I. Makarov, "Exploring efficiency of vision transformers for self-supervised monocular depth estimation," in *2022 IEEE International Symposium on Mixed and Augmented Reality (ISMAR)*. IEEE, 2022, pp. 711–719.
- [25] M. Ramamonjisoa, M. Firman, J. Watson, V. Lepetit, and D. Turmukhambetov, "Single image depth prediction with wavelet decomposition," in *Proceedings of the IEEE/CVF conference on computer vision and pattern recognition*, 2021, pp. 11 089–11 098.
- [26] J. Zhou, Y. Wang, K. Qin, and W. Zeng, "Moving indoor: Unsupervised video depth learning in challenging environments," in *Proceedings of the IEEE/CVF international conference on computer vision*, 2019, pp. 8618–8627.
- [27] Z. Yu, L. Jin, and S. Gao, "P 2 net: Patch-match and plane-regularization for unsupervised indoor depth estimation," in *European Conference on Computer Vision*. Springer, 2020, pp. 206–222.
- [28] J.-W. Bian, H. Zhan, N. Wang, T.-J. Chin, C. Shen, and I. Reid, "Auto-rectify network for unsupervised indoor depth estimation," *IEEE transactions on pattern analysis and machine intelligence*, vol. 44, no. 12, pp. 9802–9813, 2021.
- [29] C. Zhao, M. Poggi, F. Tosi, L. Zhou, Q. Sun, Y. Tang, and S. Mattoccia, "Gasmono: Geometry-aided self-supervised monocular depth estimation for indoor scenes," in *Proceedings of the IEEE/CVF International Conference on Computer Vision*, 2023, pp. 16 209–16 220.
- [30] A. Wong, X. Fei, S. Tsuei, and S. Soatto, "Unsupervised depth completion from visual inertial odometry," *IEEE Robotics and Automation Letters*, vol. 5, no. 2, pp. 1899–1906, 2020.
- [31] A. Wong and S. Soatto, "Unsupervised depth completion with calibrated backprojection layers," in *Proceedings of the IEEE/CVF International Conference on Computer Vision*, 2021, pp. 12 747–12 756.
- [32] J. Choi, D. Jung, Y. Lee, D. Kim, D. Manocha, and D. Lee, "Selfdeco: Self-supervised monocular depth completion in challenging indoor environments," in *2021 IEEE international conference on robotics and automation (icra)*. IEEE, 2021, pp. 467–474.
- [33] J. Uhrig, N. Schneider, L. Schneider, U. Franke, T. Brox, and A. Geiger, "Sparsity invariant cnns," in *2017 international conference on 3D Vision (3DV)*. IEEE, 2017, pp. 11–20.
- [34] H. Su, V. Jampani, D. Sun, O. Gallo, E. Learned-Miller, and J. Kautz, "Pixel-adaptive convolutional neural networks," in *Proceedings of the IEEE/CVF Conference on Computer Vision and Pattern Recognition*, 2019, pp. 11 166–11 175.
- [35] T. Y. Liu, P. Agrawal, A. Chen, B.-W. Hong, and A. Wong, "Monitored distillation for positive congruent depth completion," in *European Conference on Computer Vision*. Springer, 2022, pp. 35–53.
- [36] B. Mildenhall, P. P. Srinivasan, M. Tancik, J. T. Barron, R. Ramamoorthi, and R. Ng, "Nerf: Representing scenes as neural radiance fields for view synthesis," *Communications of the ACM*, vol. 65, no. 1, pp. 99–106, 2021.
- [37] K. He, X. Zhang, S. Ren, and J. Sun, "Deep residual learning for image recognition," in *Proceedings of the IEEE conference on computer vision and pattern recognition*, 2016, pp. 770–778.
- [38] J. Deng, W. Dong, R. Socher, L.-J. Li, K. Li, and L. Fei-Fei, "Imagenet: A large-scale hierarchical image database," in *2009 IEEE conference on computer vision and pattern recognition*. Ieee, 2009, pp. 248–255.
- [39] M. Jaderberg, K. Simonyan, A. Zisserman, *et al.*, "Spatial transformer networks," *Advances in neural information processing systems*, vol. 28, 2015.
- [40] Z. Wang, A. C. Bovik, H. R. Sheikh, and E. P. Simoncelli, "Image quality assessment: from error visibility to structural similarity," *IEEE transactions on image processing*, vol. 13, no. 4, pp. 600–612, 2004.

- [41] C. Wang, J. M. Buenaposada, R. Zhu, and S. Lucey, "Learning depth from monocular videos using direct methods," in *Proceedings of the IEEE conference on computer vision and pattern recognition*, 2018, pp. 2022–2030.
- [42] C. R. Givens and R. M. Shortt, "A class of wasserstein metrics for probability distributions," *Michigan Mathematical Journal*, vol. 31, no. 2, pp. 231–240, 1984.
- [43] B. Graham and L. van der Maaten, "Submanifold sparse convolutional networks," *arXiv preprint arXiv:1706.01307*, 2017.
- [44] S. Contributors, "Spconv: Spatially sparse convolution library," <https://github.com/traveller59/spconv>, 2022.
- [45] B. J. Frey and D. Dueck, "Clustering by passing messages between data points," *science*, vol. 315, no. 5814, pp. 972–976, 2007.
- [46] T.-W. Ke, J.-J. Hwang, Z. Liu, and S. X. Yu, "Adaptive affinity fields for semantic segmentation," in *Proceedings of the European conference on computer vision (ECCV)*, 2018, pp. 587–602.
- [47] A. Vaswani, "Attention is all you need," *Advances in Neural Information Processing Systems*, 2017.
- [48] N. Silberman, D. Hoiem, P. Kohli, and R. Fergus, "Indoor segmentation and support inference from rgbd images," in *Computer Vision—ECCV 2012: 12th European Conference on Computer Vision, Florence, Italy, October 7–13, 2012, Proceedings, Part V 12*. Springer, 2012, pp. 746–760.
- [49] A. Paszke, S. Gross, F. Massa, A. Lerer, J. Bradbury, G. Chanan, T. Killeen, Z. Lin, N. Gimelshein, L. Antiga, *et al.*, "Pytorch: An imperative style, high-performance deep learning library," *Advances in neural information processing systems*, vol. 32, 2019.
- [50] D. P. Kingma, "Adam: A method for stochastic optimization," *arXiv preprint arXiv:1412.6980*, 2014.
- [51] S. F. Bhat, I. Alhashim, and P. Wonka, "Adabins: Depth estimation using adaptive bins," in *Proceedings of the IEEE/CVF conference on computer vision and pattern recognition*, 2021, pp. 4009–4018.
- [52] A. Dai, A. X. Chang, M. Savva, M. Halber, T. Funkhouser, and M. Nießner, "Scannet: Richly-annotated 3d reconstructions of indoor scenes," in *Proceedings of the IEEE conference on computer vision and pattern recognition*, 2017, pp. 5828–5839.
- [53] P. Ji, R. Li, B. Bhanu, and Y. Xu, "Monoindoor: Towards good practice of self-supervised monocular depth estimation for indoor environments," in *Proceedings of the IEEE/CVF international conference on computer vision*, 2021, pp. 12 787–12 796.
- [54] L. Yang, B. Kang, Z. Huang, X. Xu, J. Feng, and H. Zhao, "Depth anything: Unleashing the power of large-scale unlabeled data," in *Proceedings of the IEEE/CVF Conference on Computer Vision and Pattern Recognition*, 2024, pp. 10 371–10 381.
- [55] B. Ke, A. Obukhov, S. Huang, N. Metzger, R. C. Daudt, and K. Schindler, "Repurposing diffusion-based image generators for monocular depth estimation," in *Proceedings of the IEEE/CVF Conference on Computer Vision and Pattern Recognition (CVPR)*, 2024.
- [56] H. Lin, S. Peng, J. Chen, S. Peng, J. Sun, M. Liu, H. Bao, J. Feng, X. Zhou, and B. Kang, "Prompting depth anything for 4k resolution accurate metric depth estimation," *arXiv preprint arXiv:2412.14015*, 2024.